SANDIA REPORT
SAND2012-10686
Unlimited Release
Printed December 2012

Forming Rotated SAR Images by Real-Time Motion Compensation

Armin W. Doerry

Prepared by
Sandia National Laboratories
Albuquerque, New Mexico 87185 and Livermore, California 94550

Sandia National Laboratories is a multi-program laboratory managed and operated by Sandia Corporation, a wholly owned subsidiary of Lockheed Martin Corporation, for the U.S. Department of Energy's National Nuclear Security Administration under contract DE-AC04-94AL85000.

Approved for public release; further dissemination unlimited.

Sandia National Laboratories

Issued by Sandia National Laboratories, operated for the United States Department of Energy by Sandia Corporation.

NOTICE: This report was prepared as an account of work sponsored by an agency of the United States Government. Neither the United States Government, nor any agency thereof, nor any of their employees, nor any of their contractors, subcontractors, or their employees, make any warranty, express or implied, or assume any legal liability or responsibility for the accuracy, completeness, or usefulness of any information, apparatus, product, or process disclosed, or represent that its use would not infringe privately owned rights. Reference herein to any specific commercial product, process, or service by trade name, trademark, manufacturer, or otherwise, does not necessarily constitute or imply its endorsement, recommendation, or favoring by the United States Government, any agency thereof, or any of their contractors or subcontractors. The views and opinions expressed herein do not necessarily state or reflect those of the United States Government, any agency thereof, or any of their contractors.

Printed in the United States of America. This report has been reproduced directly from the best available copy.

Available to DOE and DOE contractors from

U.S. Department of Energy
Office of Scientific and Technical Information
P.O. Box 62
Oak Ridge, TN 37831

Telephone: (865) 576-8401
Facsimile: (865) 576-5728
E-Mail: reports@adonis.osti.gov
Online ordering: http://www.osti.gov/bridge

Available to the public from

U.S. Department of Commerce
National Technical Information Service
5285 Port Royal Rd.
Springfield, VA 22161

Telephone: (800) 553-6847
Facsimile: (703) 605-6900
E-Mail: orders@ntis.fedworld.gov
Online order: http://www.ntis.gov/help/ordermethods.asp?loc=7-4-0#online

SAND2012-10686
Unlimited Release
Printed December 2012

Forming Rotated SAR Images by Real-Time Motion Compensation

Armin W. Doerry
ISR Mission Engineering
Sandia National Laboratories
Albuquerque, NM 87185-0519

Abstract

Proper waveform parameter selection allows collecting Synthetic Aperture Radar (SAR) phase history data on a rotated grid in the Fourier Space of the scene being imaged. Subsequent image formation preserves the rotated geometry to allow SAR images to be formed at arbitrary rotation angles without the use of computationally expensive interpolation or resampling operations. This should be useful where control of image orientation is desired such as generating squinted stripmaps and VideoSAR applications, among others.

Acknowledgements

The updated production of this report is a result of an unfunded Internal Research and Development effort.

Contents

Foreword 6

Introduction 7

Background 9

Forming a Rotated SAR Image 12

Simulations 19

Discussion and Conclusions 23

References 25

Foreword

This report is an updated and enhanced version of a previous limited distribution report [“Forming Rotated SAR Images by Real-time Motion Compensation”, Sandia Report SAND 2001-1740P, Internal Distribution Only]. The distribution limitation of the earlier report was merely because of the publication vehicle being an Internal Memorandum, chosen at the time arbitrarily, with no other particular reason for restricting its Unlimited Release.

This report details the results of an academic study. It does not presently exemplify any modes, methodologies, or techniques employed by any operational system known to the authors.

The specific mathematics and algorithms presented herein do not bear any release restrictions or distribution limitations.

This distribution limitations of this report are in accordance with the classification guidance detailed in the memorandum “Classification Guidance Recommendations for Sandia Radar Testbed Research and Development”, DRAFT memorandum from Brett Remund (Deputy Director, RF Remote Sensing Systems, Electronic Systems Center) to Randy Bell (US Department of Energy, NA-22), February 23, 2004. Sandia has adopted this guidance where otherwise none has been given.

This report formalizes preexisting informal notes and other documentation on the subject matter herein.

1. Introduction

The most natural image display geometry for a Synthetic Aperture Radar (SAR) is for the image *y*-axis to be in a direction away from the SAR synthetic aperture center and through the image scene center (as projected on the ground). The *x*-axis would of course be perpendicular to this and also on the ground. With this definition, the actual squint angle employed for data collection corresponds to the orientation of the synthetic aperture itself, which is irrelevant to the image orientation (layover effects notwithstanding), since only the aperture center and scene center define the image orientation.

However, occasions exist where it would be useful to rotate the image to a new orientation, where the physical directions of the *x* and *y* axes do not depend on the location of the aperture center. While rotations of multiples of 90 degrees are trivial, arbitrary rotations are considerably more difficult. The following list presents some applications and other reasons for such a capability,

- forming a squinted stripmap in a “push-broom” fashion,
- maintaining constant scene orientation for Video-SAR,
- creating conventional “North-up” maps,
- creating registered image pairs for easier stereoscopic analysis, and
- some customers just want it that way.[1,2]

Some of these are illustrated in figure 1.

Typically, a reoriented SAR image is first formed in the most natural way as described above, and then rotated by resampling to a new grid. This is computationally expensive and prone to image distortion from inadequate interpolators, especially if the image is complex (with I and Q values).

The confluence of several ideas indicate how an arbitrarily oriented SAR image may be formed without overt image interpolations. These are

- the recognition that a translation in Fourier space is equivalent to a linear phase change in the image,
- the recognition that *any* area in the Fourier space of the scene will render an image of the scene,
- the recognition that a rotated image scene will have a similarly rotated Fourier space representation, consequently rotating the Fourier space of a scene will allow forming rotated images, and
- the unprecedented ability to accurately place phase history data samples in Fourier space with great control via real-time motion compensation with high-performance waveform generators and radar timing.

The remainder of this report will discuss how this might be achieved.

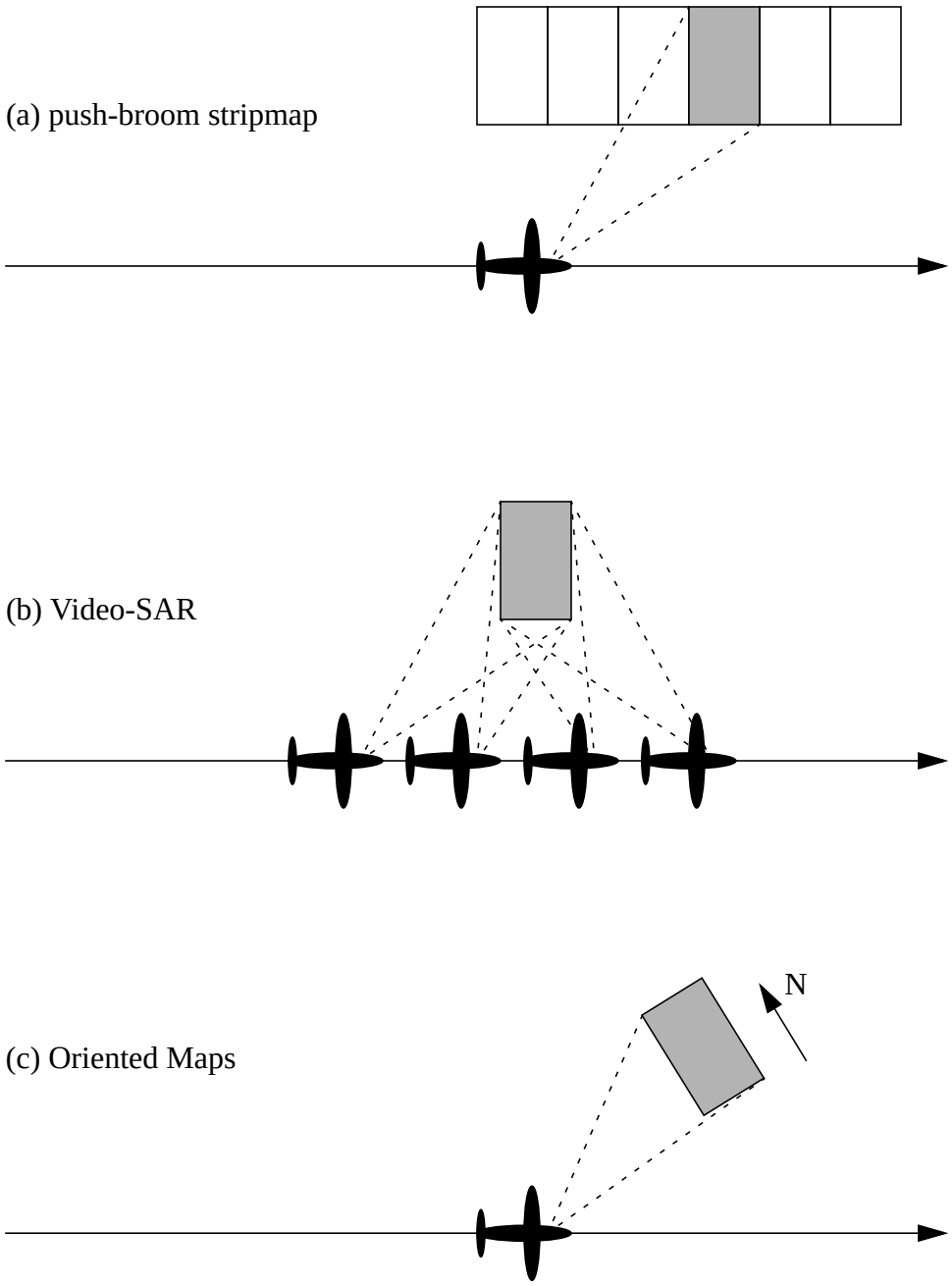

Figure 1. Useful applications for rotated images.

2. Background

We begin with a brief reintroduction of basic SAR imaging concepts of an unrotated scene, largely taken from an earlier report.[3]

Consider a 3-D world with the radar geometry of figure 2. In this geometry we define

$\boldsymbol{s}$ = the spatial location of a point target, with coordinates (s_x, s_y, s_z),
$\boldsymbol{r}_c$ = the location of the radar, with coordinates (r_x, r_y, r_z), and
$\boldsymbol{r}_s = \boldsymbol{r}_c - \boldsymbol{s}$ = relation of radar location to the point target location. (1)

We will presume a linear frequency modulated (LFM) transmitted pulse given by

$$X_T(t, n) = A_T \mathrm{rect}\left(\frac{t}{T}\right)\cos\left(\omega_n t + \frac{\gamma_n}{2}t^2\right). \tag{2}$$

where

ω_n = center frequency of the transmitted pulse,
γ_n = chirp rate of the transmitted pulse,
n = an index of pulse number such that $-\frac{N}{2} \le n \le \frac{N}{2} - 1$
A_T = amplitude of the transmitted pulse, and
T = duration of transmitted pulse. (3)

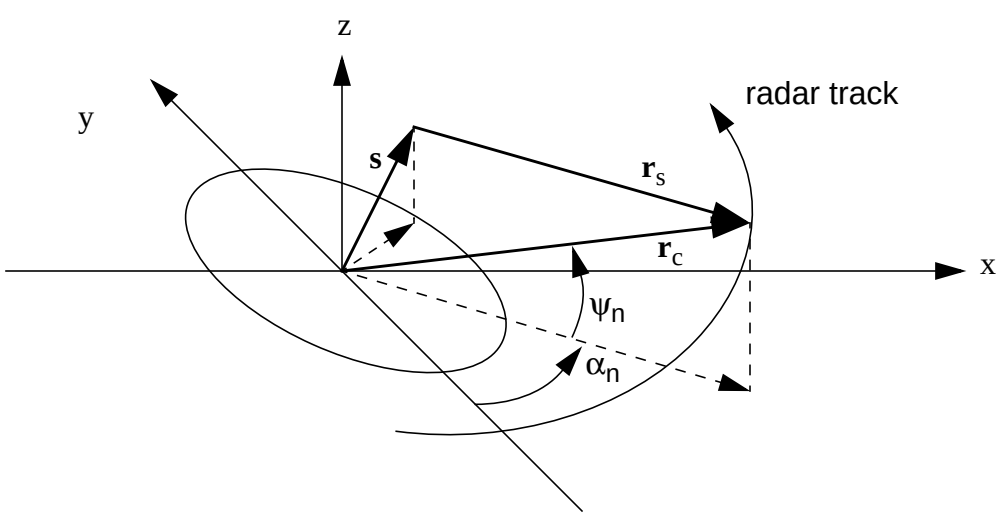

Figure 2. Data collection geometry in a 3-D world.

The received echo will be a scaled and time delayed version of the transmitted signal, namely

$$X_R(t, n) \;=\; \frac{A_R}{A_T}\sigma(\boldsymbol{s})X_T(t-t_s) \;=\; A_R\sigma(\boldsymbol{s})\mathrm{rect}\left(\frac{t-t_s}{T}\right)\cos\left(\omega_n(t-t_s) + \frac{\gamma_n}{2}(t-t_s)^2\right), \tag{4}$$

where

A_R is the nominal amplitude of the received echo, and
$\sigma(\boldsymbol{s})$ is the reflectivity of the target at $\boldsymbol{s}$. (5)

The echo delay time with respect to the target depends on the distance to the target and the speed of wave propagation, and is

$$t_s \;=\; \frac{2}{c}|\boldsymbol{r}_s|\,. \tag{6}$$

The echo delay time with respect to the scene center is given by

$$t_c \;=\; \frac{2}{c}|\boldsymbol{r}_c|\,. \tag{7}$$

De-chirping this (stretch processing) and using quadrature demodulation yields a video signal of the approximate form

$$X_V(t, n) \approx A_R\sigma(\boldsymbol{s})\mathrm{rect}\left(\frac{t-t_c}{T}\right)\exp j\{\omega_n(t_c-t_s) + \gamma_n(t-t_c)(t_c-t_s)\}\,. \tag{8}$$

We are ignoring the residual video phase error term. If we completely sample this interval with an Analog to Digital converter at times

$$(t-t_c) \;=\; iT_s \tag{9}$$

where

i = sample index such that $-\frac{I}{2} \le i \le \frac{I}{2} - 1$, and
$T_s = T/I$ = ADC sample spacing, (10)

then the sampled video signal becomes

$$X_V(i, n) \approx A_R\sigma(\boldsymbol{s})\exp j\{[\omega_n + \gamma_n T_s i](t_c-t_s)\}\,. \tag{11}$$

Note that each sample index i represents a different instantaneous frequency $[\omega_n + \gamma_n T_s i]$.

The time difference quantity $(t_c - t_s)$ can be related to ranges and expanded to

$$(t_c-t_s) \approx \frac{2}{c}(s_x\cos\psi_n\sin\alpha_n - s_y\cos\psi_n\cos\alpha_n + s_z\sin\psi_n)\,. \tag{12}$$

This expression does ignore some higher-order error terms that account for wavefront

curvature, but is sufficient for the task at hand. Typically we also assume $s_z = 0$. Nevertheless, this can be inserted into the video signal expression and rearranged to

$$X_V(i,n) \approx A_R \sigma(\boldsymbol{s}) \exp j\left\{\frac{2}{c}[\omega_n + \gamma_n T_s i]\cos\psi_n(s_x \sin\alpha_n - s_y \cos\alpha_n)\right\}. \tag{13}$$

The subscript index *n* reflects the quantities that can (including those that we allow to) change from pulse to pulse during a data collection (synthetic aperture). This model is reasonably accurate over small scenes (compared to range).

The usual and customary presumption has been that $\alpha_0 = 0$, which implies that the y-axis runs beneath the synthetic aperture center. A natural image display after processing by any of a variety of algorithms would typically be as illustrated in figure 3.

The question now is “What about a rotated image?”

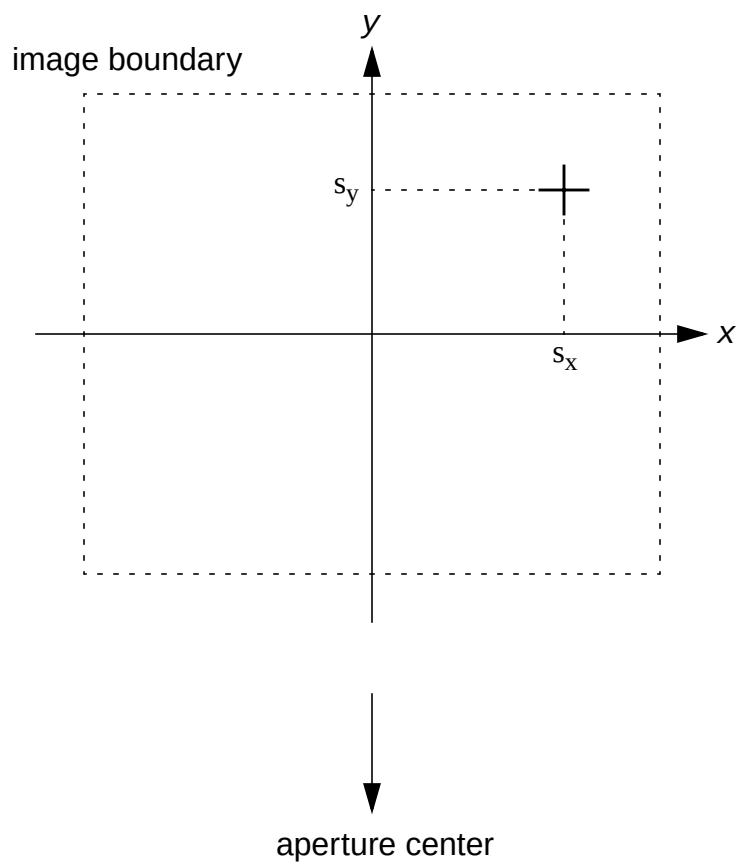

Figure 3. Typical image orientation.

3. Forming a Rotated SAR Image

Consider the coordinates of a target location in a rotated image geometry, as illustrated in figure 4. in the primed coordinate frame we observe the following

$$
\begin{aligned}
s_x' &= s_x \cos\alpha_R + s_y \sin\alpha_R \\
s_y' &= -s_x \sin\alpha_R + s_y \cos\alpha_R
\end{aligned}
\tag{14}
$$

and furthermore

$$
\begin{aligned}
s_x &= s_x' \cos\alpha_R - s_y' \sin\alpha_R \\
s_y &= s_x' \sin\alpha_R + s_y' \cos\alpha_R
\end{aligned}
\tag{15}
$$

where α_R is the desired rotation angle.

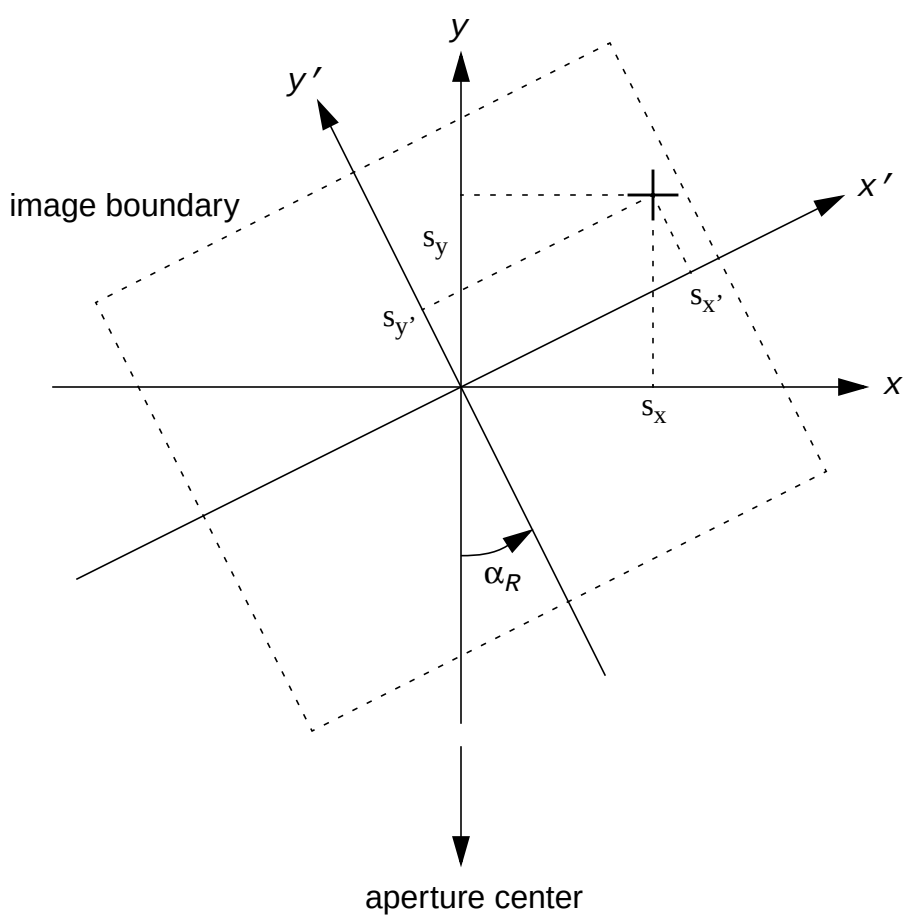

Figure 4. Rotated image geometry definitions.

Plugging this into the equation for the video data yields

$$X_V(i,n) \approx A_R \sigma(\boldsymbol{s}) \exp j\left\{\frac{2}{c}[\omega_n + \gamma_n T_s i]\cos\psi_n \begin{pmatrix} (s_x'\cos\alpha_R - s_y'\sin\alpha_R)\sin\alpha_n \\ -(s_x'\sin\alpha_R + s_y'\cos\alpha_R)\cos\alpha_n \end{pmatrix}\right\} \tag{16}$$

which can be simplified to

$$X_V(i,n) \approx A_R \sigma(\boldsymbol{s}) \exp j\left\{\frac{2}{c}[\omega_n + \gamma_n T_s i]\cos\psi_n \begin{pmatrix} s_x'\sin(\alpha_n - \alpha_R) \\ -s_y'\cos(\alpha_n - \alpha_R) \end{pmatrix}\right\}. \tag{17}$$

Clearly, the rotated image coordinate frame is tantamount to collecting phase history data *NOT* centered over the y' axis, but with some angular offset.

3.1. Real-time Motion Compensation

Now consider adjusting SAR chirp waveform parameters such that

$$[\omega_n + \gamma_n T_s i]\cos\psi_n \cos(\alpha_n - \alpha_R) \;=\; [\omega_0 + \gamma_0 T_s i]\cos\psi_0 \cos\alpha_R . \tag{18}$$

This might be accomplished by setting

$$\omega_n \;=\; \omega_0\left(\frac{\cos\psi_0\cos\alpha_R}{\cos\psi_n\cos(\alpha_n - \alpha_R)}\right), \text{ and}$$

$$\gamma_n \;=\; \gamma_0\left(\frac{\cos\psi_0\cos\alpha_R}{\cos\psi_n\cos(\alpha_n - \alpha_R)}\right) \tag{19}$$

although adjusting ADC sampling times and rates could also achieve this.

In either case, such adjustments allow the data to be modeled by

$$X_V(i,n) \approx A_R \sigma(\boldsymbol{s}) \exp j\left\{\frac{2}{c}[\omega_0 + \gamma_0 T_s i]\cos\psi_0 \cos\alpha_R \begin{pmatrix} s_x'\tan(\alpha_n - \alpha_R) \\ -s_y' \end{pmatrix}\right\}. \tag{20}$$

We select sampling positions such that

$$\tan(\alpha_n - \alpha_R) \;=\; d\alpha\, n - \tan\alpha_R \tag{21}$$

which forces

$$\alpha_n \;=\; \operatorname{atan}(d\alpha\, n - \tan\alpha_R) + \alpha_R . \tag{22}$$

Doing so allows the phase history data to be modeled by

$$X_V(i,n) \approx A_R \sigma(\boldsymbol{s}) \exp j\left\{ \frac{2}{c}[\omega_0 + \gamma_0 T_s i] \cos\psi_0 \cos\alpha_R \begin{pmatrix} s_x' d\alpha\, n - s_y' \\ -s_x' \tan\alpha_R \end{pmatrix} \right\}. \tag{23}$$

The only real pesky term here is $s_x' \tan\alpha_R$ which geometrically warps the image. However, signal processing can remove this, as we shall see shortly.

In the Fourier space of the rotated scene, the phase history data sample locations describe an aperture that is offset from the k_y' axis, but still somewhat oriented with the k_x' axis, as illustrated in figure 5.

Note: The shape of the entire aperture in Fourier space indicates that if we use the entire data set without cropping, then we can expect the sidelobe structure to be dependent on α_R. While cropping the Fourier space could control sidelobe dependence on α_R, losing Fourier space data would necessarily coarsen the resolution as well.[4]

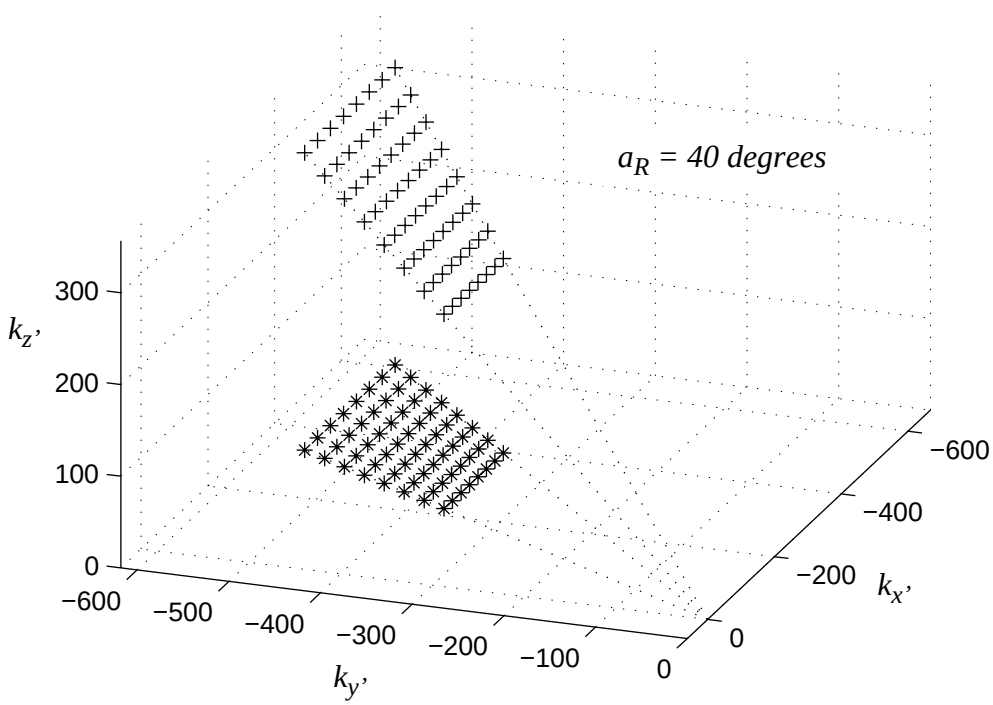

Figure 5. Locations of motion compensated data in Fourier space of rotated image.

3.2. Image Formation

Following the lead of the earlier report, we employ Polar Format processing using the Chirped Z-Transform (CZT).[3]

3.2.1. Azimuth Processing using CZT

We apply the CZT to achieve the first intermediate processing goal as follows

$$
\begin{aligned}
X_1(i,u) &= CZT_n\{X_V(i,n)\} \\
&\approx \left[\begin{array}{c} A_R\sigma(\boldsymbol{s})\exp j\left\{-\frac{2}{c}[\omega_0+\gamma_0 T_s i]\cos\psi_0\cos\alpha_R(s_y'+s_x'\tan\alpha_R)\right\} \\ \times\sum_n \left(e^{j\left\{\frac{2\omega_0\cos\psi_0\cos\alpha_R}{c}d\alpha s_x'\left(1+\frac{\gamma_0 T_s}{\omega_0}i\right)n\right\}} \right) e^{-j\Delta_f un} \end{array} \right] \\
&\approx \left[\begin{array}{c} A_R\sigma(\boldsymbol{s})\exp j\left\{-\frac{2}{c}[\omega_0+\gamma_0 T_s i]\cos\psi_0\cos\alpha_R(s_y'+s_x'\tan\alpha_R)\right\} \\ \times\sum_n \left(e^{j\left\{\frac{2\omega_0\cos\psi_0\cos\alpha_R}{c}d\alpha s_x'\left(1+\frac{\gamma_0 T_{s,0}}{\omega_0}i\right)-\Delta_f u\right\}n} \right) \end{array} \right].
\end{aligned}
\tag{24}
$$

If we force Δ_f to vary with index i, that is we scale frequency spacing to

$$
\Delta_f = \frac{2\pi}{N}\left(1+\frac{\gamma_0 T_s}{\omega_0}i\right) \tag{25}
$$

then we have

$$
X_1(i,u) \approx \left[\begin{array}{c} A_R\sigma(\boldsymbol{s})\exp j\left\{-\frac{2}{c}[\omega_0+\gamma_0 T_s i]\cos\psi_0\cos\alpha_R(s_y'+s_x'\tan\alpha_R)\right\} \\ \times\sum_n \left(e^{j\left(1+\frac{\gamma_0 T_{s,0}}{\omega_0}i\right)\left\{\frac{2\omega_0\cos\psi_0\cos\alpha_R}{c}d\alpha s_x'-\frac{2\pi}{N}u\right\}n} \right) \end{array} \right]. \tag{26}
$$

Performing the summation yields

$$X_1(i,u) \approx \left[\begin{array}{l} A_R \sigma(\boldsymbol{s}) \exp j\left\{ -\frac{2}{c}[\omega_0 + \gamma_0 T_s i] \cos\psi_0 \cos\alpha_R (s_y' + s_x' \tan\alpha_R) \right\} \\ \times W_n\left(\left(1 + \frac{\gamma_0 T_{s,0}}{\omega_0} i\right) \left\{ \frac{2\omega_0 \cos\psi_0 \cos\alpha_R}{c} d\alpha s_x' - \frac{2\pi}{N} u \right\} \right) \end{array} \right] \tag{27}$$

where the impulse response shape is given by

$$W_n(\Omega) = \sum_n e^{j\Omega n}. \tag{28}$$

This clearly offers a peak response when

$$\frac{2\pi}{N} u = \frac{2\omega_0 \cos\psi_0 \cos\alpha_R}{c} d\alpha s_x' \tag{29}$$

with location that is independent of index *i*. This allows us to estimate s_x' as

$$s_x' \approx \frac{2\pi}{N}\left(\frac{c}{2\omega_0 \cos\psi_0 \cos\alpha_R d\alpha}\right) u. \tag{30}$$

To complete the image formation, we need to transform across index *i*. But first we need to correct for the problematic $s_x' \tan\alpha_R$ term.

Azimuth Resolution

We note that the concept of azimuth resolution is somewhat altered by this processing, and now depends on $\cos\alpha_R$. Specifically, azimuth resolution is calculated to be nominally

$$\rho_x' = \frac{\lambda_0}{2N d\alpha \cos\psi_0 \cos\alpha_R} \tag{31}$$

where nominal wavelength $\lambda_0 = 2\pi c / \omega_0$.

This indicates a coarsening of resolution as α_R departs from 0. This could be accommodated by increasing *N* correspondingly.

3.2.2. Warp Error Correction

We now have the information that we need to correct the problematic warping. We do this by correcting each partially processed data sample in $X_1(i, u)$ with a phase error correction term given by

$$\exp j\left\{\frac{2}{c}[\omega_0 + \gamma_0 T_s i]\cos\psi_0 \sin\alpha_R s_x'\right\}. \tag{32}$$

Consequently, the corrected data is given by

$$\begin{aligned} X_2(i, u) &= X_1(i, u)\exp j\left\{\frac{2}{c}[\omega_0 + \gamma_0 T_s i]\cos\psi_0 \sin\alpha_R s_x'\right\} \\ &\approx \left[\begin{array}{l} A_R\sigma(\boldsymbol{s})\exp j\left\{-\frac{2}{c}[\omega_0 + \gamma_0 T_s i]\cos\psi_0 \cos\alpha_R s_y'\right\} \\ \times W_n\left(\left(1 + \frac{\gamma_0 T_{s,0}}{\omega_0} i\right)\left\{\frac{2\omega_0\cos\psi_0\cos\alpha_R}{c} d\alpha s_x' - \frac{2\pi}{N}u\right\}\right) \end{array}\right] \end{aligned} \tag{33}$$

which can be rearranged to

$$\begin{aligned} X_2(i, u) &\approx \left[\begin{array}{l} A_R\sigma(\boldsymbol{s})W_n\left(\left(1 + \frac{\gamma_0 T_{s,0}}{\omega_0} i\right)\left\{\frac{2\omega_0\cos\psi_0\cos\alpha_R}{c} d\alpha s_x' - \frac{2\pi}{N}u\right\}\right) \\ \times \exp j\left\{-\frac{2}{c}[\omega_0 + \gamma_0 T_s i]\cos\psi_0 \cos\alpha_R s_y'\right\} \end{array}\right] \\ &\approx \left[\begin{array}{l} A_R\exp j\left\{-\frac{2}{c}\omega_0\cos\psi_0\cos\alpha_R s_y'\right\}\sigma(\boldsymbol{s}) \\ \times W_n\left(\frac{2\omega_0\cos\psi_0\cos\alpha_R}{c} d\alpha s_x' - \frac{2\pi}{N}u\right) \\ \times \exp j\left\{-\frac{2}{c}[\gamma_0 T_s i]\cos\psi_0 \cos\alpha_R s_y'\right\} \end{array}\right]. \end{aligned} \tag{34}$$

if we ignore the inconsequential fluctuation in the width of the azimuth IPR due to index *i*. Note that the phase is linear in index i.

3.2.3. Range Processing with FFT

Performing a FFT across index *i* yields

$$FFT_i\{X_2(i,u)\} = \sum_i X_2(i,u)e^{-j\frac{2\pi}{I}vi}$$

$$\approx \left[\begin{array}{l} A_R \exp j\left\{-\frac{2}{c}\omega_0 \cos\psi_0 \cos\alpha_R s_y'\right\}\sigma(\boldsymbol{s}) \\ \times W_n\left(\frac{2\omega_0 \cos\psi_0 \cos\alpha_R}{c} d\alpha s_x' - \frac{2\pi}{N}u\right) \\ \times \sum_i e^{-j\left\{\frac{2}{c}\gamma_0 T_s \cos\psi_0 \cos\alpha_R s_y' + \frac{2\pi}{I}v\right\}i} \end{array}\right] \tag{35}$$

$$\approx \left[\begin{array}{l} A_R \exp j\left\{-\frac{2}{c}\omega_0 \cos\psi_0 \cos\alpha_R s_y'\right\}\sigma(\boldsymbol{s}) \\ \times W_n\left(\frac{2\omega_0 \cos\psi_0 \cos\alpha_R}{c} d\alpha s_x' - \frac{2\pi}{N}u\right) \\ \times W_i\left(\frac{2}{c}\gamma_0 T_s \cos\psi_0 \cos\alpha_R s_y' + \frac{2\pi}{I}v\right) \end{array}\right].$$

This represents the 2-D complex IPR of a point target in a 3-D geometry, and clearly offers a peak response when

$$\frac{2\pi}{I}v = -\frac{2}{c}\gamma_0 T_s \cos\psi_0 \cos\alpha_R s_y' \tag{36}$$

as well as when

$$\frac{2\pi}{N}u = \frac{2\omega_0 \cos\psi_0 \cos\alpha_R}{c} d\alpha s_x'. \tag{37}$$

Note that the residual phase perturbation is inconsequential to a magnitude detected image, but could be compensated if so desired.

<u>*Range Resolution*</u>

As with azimuth resolution, ground range resolution is now coarsened to nominally

$$\rho_y' = \frac{c}{2B_{eff}\cos\psi_0 \cos\alpha_R} \tag{38}$$

where the effective bandwidth is $B_{eff} = \gamma_0 T_s I/(2\pi)$.

4. Simulations

4.1. Scene Fly-by

Consider a fly-by of a target scene as illustrated in figure 6. Successive spotlight images would normally show a rotating scene as the aircraft's aspect changed with time.

The following sequence of images are stabilized (all effectively rotated to a common orientation) using the real-time motion compensation procedure of this report. However, note the variations in the sidelobe structure.

The images simulate a nominal 1-m resolution at Ku-band, and are processed without employing any window functions so as to high-light the sidelobe structure variations as a function of α_R.

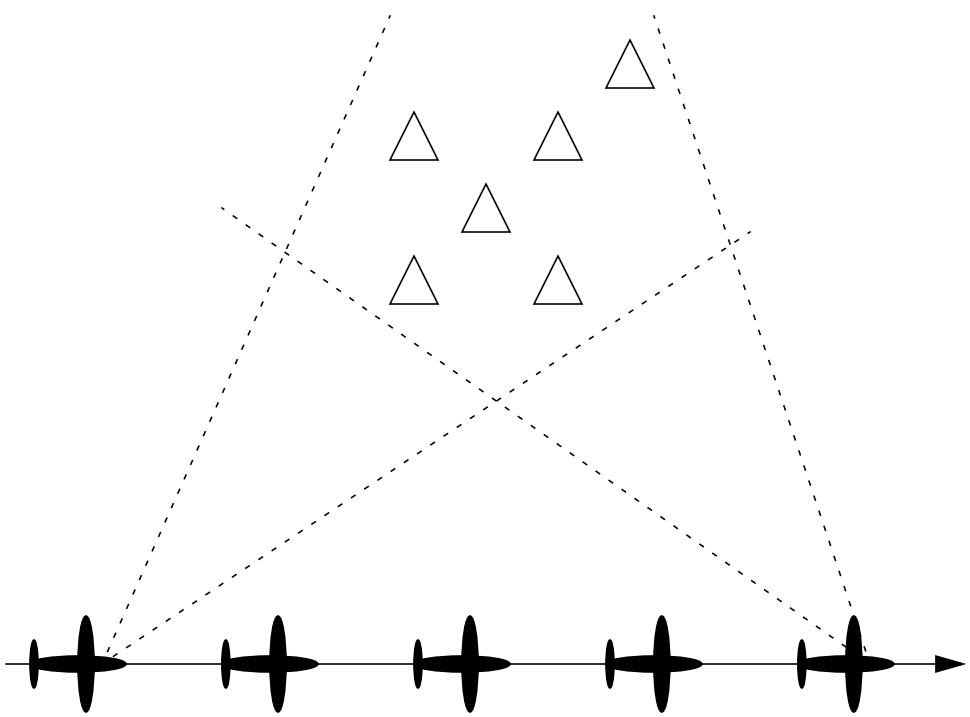

Figure 6. Illustration of scene fly-by.

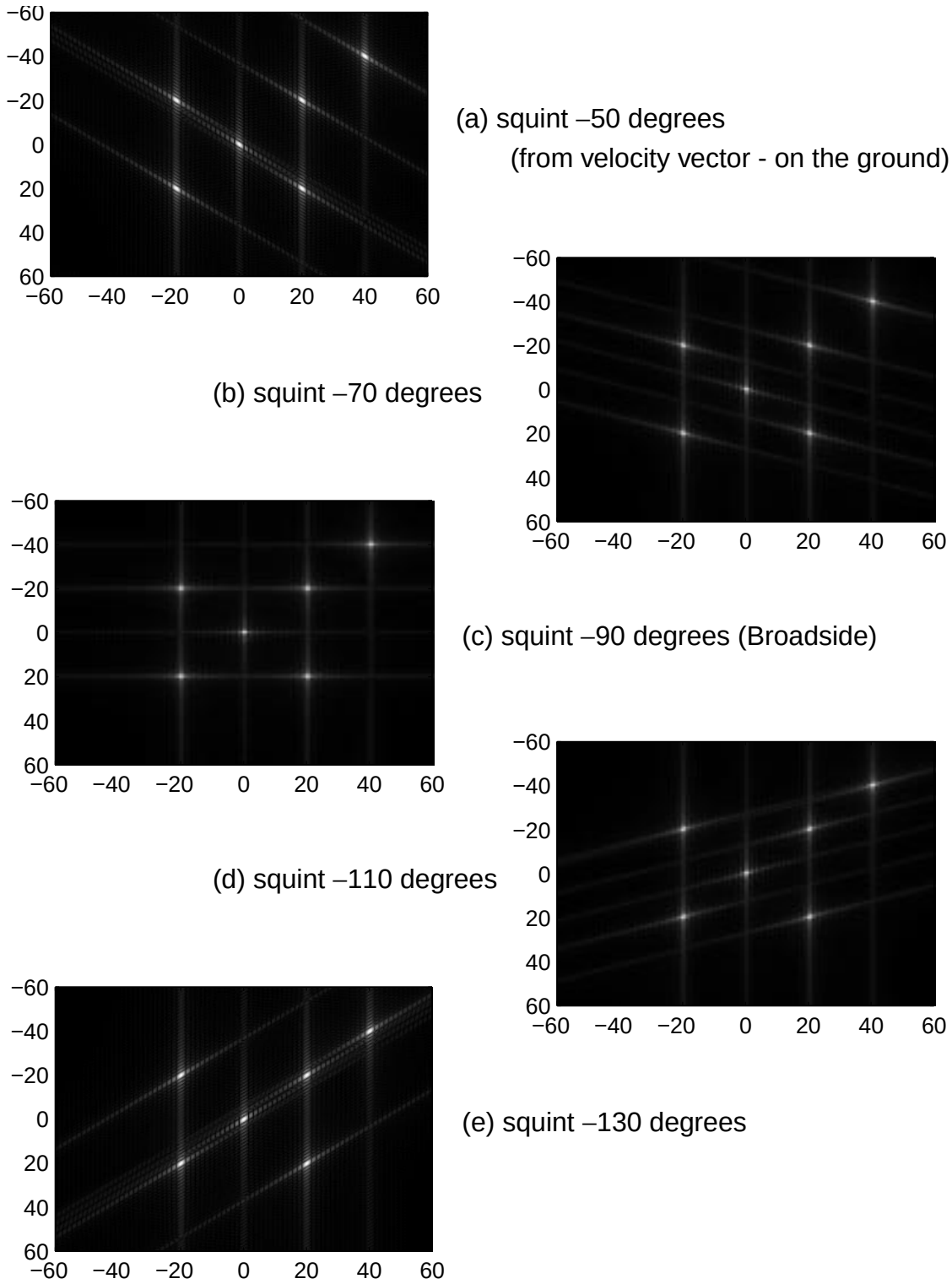

Figure 7. Simulated images from scene fly-by, rotated to common orientation using real-time motion compensation.

4.2. Scene Orientation

Consider a broadside imaging geometry of a target scene as illustrated in figure 8. Typically, the image orientation would be a broadside viewing perspective from the aircraft's position at the center of the synthetic aperture.

The following sequence of images are formed using the exact same imaging geometry. Differences in orientation are due to phase history data rotation using the real-time motion compensation procedure of this report.

The images simulate a nominal 1-m resolution at Ku-band, and are processed without employing any window functions so as to high-light the sidelobe structure variations as a function of α_R.

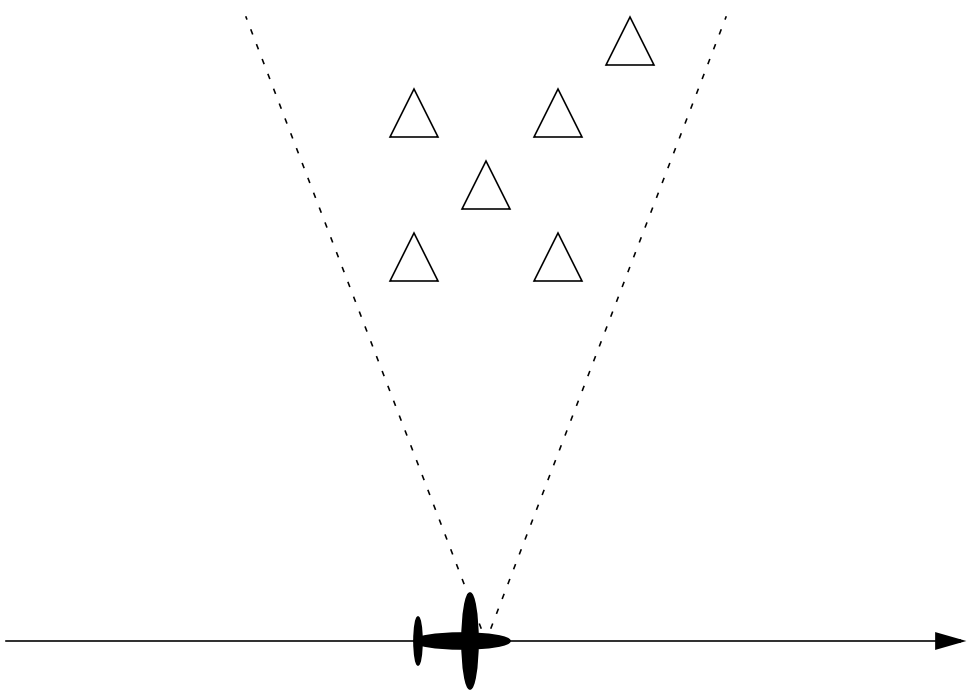

Figure 8. Broadside imaging geometry of scene.

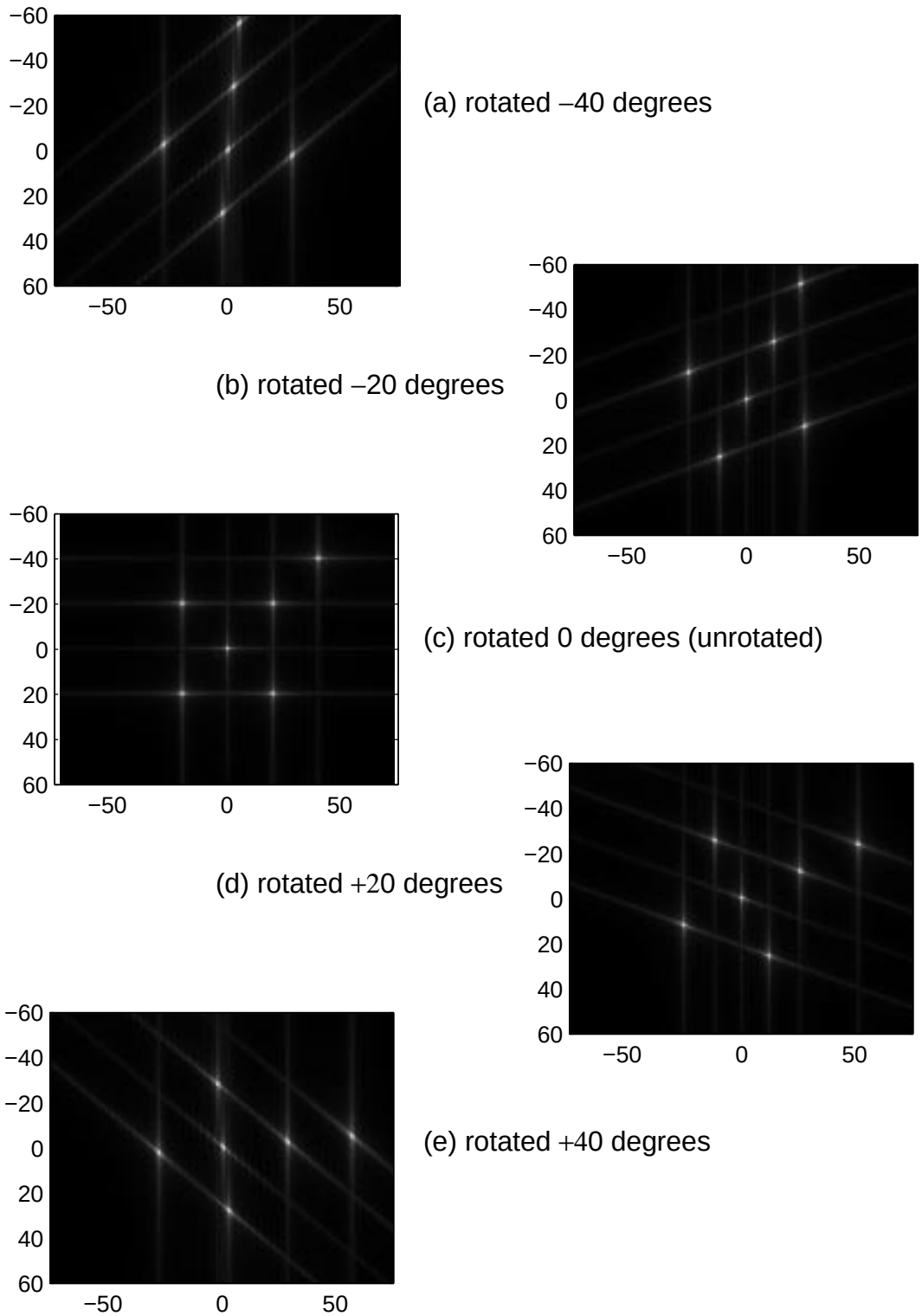

Figure 9. Simulation of effect of image rotation using different real-time motion compensation with same collection geometry.

5. Discussion and Conclusions

We observe the following.

- A variety of applications call for SAR images rotated from their ‘natural’ orientation to some other perhaps more useful orientation. Such rotation angles may not be limited to the relatively easy multiples of 90 degrees, but might need to be any real angle.
- Rotated images can be formed from rotated Fourier-space data, i.e., phase-history data.
- Proper real-time motion compensation via waveform parameter manipulation (and/or perhaps ADC sample positioning) can place Fourier-space samples on a rotated grid. This eliminates the need for computationally expensive overt data resampling or interpolation.
- Rotation angles beyond ± 45 degrees can be accomplished by combinations of a rotation angle less than ± 45 along with perhaps multiple 90-degree rotations.
- Sidelobe structure within the SAR image will, however, vary with rotation angle.
- Image resolution (in x and y directions) will coarsen proportionately with the secant of the rotation angle out to ± 45 degrees. This can, however, be compensated by increasing synthetic aperture length and data bandwidth.

“The question is not what you look at, but what you see.”
— Henry David Thoreau

6. References

[1] Harmony, D. W., “SAR Slant Planes”, memo to Distribution, Jan. 3, 1997.

[2] Harmony, D. W., “Squint, Image Import and Slant Plane Remapping”, memo to Distribution, January 24, 1997.

[3] Doerry, Armin W., “Real-time Polar-Format Processing for Sandia’s Testbed Radar Systems”, Sandia Internal Memorandum SAND2001-1644P, June 2001.

[4] Doerry, Armin W., “Trapezoidal 2-D apertures and Impulse Response”, memo to Distribution, 3 January 2000.

Distribution

Unlimited Release

1	MS 0532	J. J. Hudgens	5240	
1	MS 0519	J. A. Ruffner	5349	
1	MS 0519	A. W. Doerry	5349	
1	MS 0899	Technical Library	9536	(electronic copy)

;-)